Trans Indian Inst Met
DOI 10.1007/s12666-017-1067-0

TECHNICAL PAPER

Tensile Properties and Tensile Fracture Characteristics of Cast Al–Zn–Mg Alloys Processed by Equal Channel Angular Pressing

G. K. Manjunath[1] · G. V. Preetham Kumar[1] · K. Udaya Bhat[1]

Received: 29 November 2016 / Accepted: 6 February 2017

Abstract In the present work, as-cast Al–5Zn–2Mg, Al–10Zn–2Mg and Al–15Zn–2Mg alloys were ECAP processed and tensile tests were carried out to determine the strength and ductility. After tensile testing, morphology of the fracture surfaces of tensile tested samples were studied. After ECAP processing, significant improvement in the yield stress and ultimate tensile strength were observed in all the three alloys. Also, yield stress and ultimate tensile strength were increased with increase in the zinc content of the material. The elongation to failure increased significantly with increase in the number of ECAP passes. SEM micrographs revealed that, the fracture surface of the cast samples of the alloys were composed of the dendritic structure, while the ECAP processed samples consisted of small size dimples. Size of the dimples were reduced with the increase in the number of ECAP passes.

Keywords ECAP · Al–Zn–Mg alloy · Ultimate tensile strength · Elongation to failure · Fracture morphology

✉ G. K. Manjunath
manjugk2001@gmail.com

G. V. Preetham Kumar
pkphd@hotmail.com

K. Udaya Bhat
udayabhatk@gmail.com

[1] Department of Metallurgical and Materials Engineering, National Institute of Technology Karnataka, Surathkal, Mangalore 575025, India

1 Introduction

The materials with ultrafine grain (UFG) size developed through severe plastic deformation (SPD) methods have received great interest in the last decade because of their significant properties [1]. Equal channel angular pressing (ECAP) is considered as the most promising and potential technique amongst other SPD techniques because of its simplicity [2]. ECAP was first introduced by Segal in 1981 [3], later on numerous researches have been reported on various metallic materials. In ECAP process, materials are subjected to shear deformation which induces large plastic strain in the materials. In ECAP process, cross-section of the sample remains unchanged after processing, so that the samples can be pressed over and over again to achieve a very large plastic strain [4]. Aluminium and its alloys have been used for many years in engineering applications due to their high strength to weight ratio. The Al–Zn–Mg alloys are among the most important aluminium alloys used in the aerospace, military equipments and light weight structural applications [5]. The mechanical properties of these alloys are poor in as-cast condition and there is a continuous interest to improve it through different processes.

Several works have been reported to analyse the effect of ECAP processing particularly on tensile properties of aluminium alloys. Prados et al. [6] studied the tensile properties of cast Al–4Cu alloy processed by ECAP and conventional extrusion. Due to the presence of high angle grain boundaries in ECAP processed samples, better tensile properties were observed compared to the conventionally extruded samples. The fracture mode was changed from the brittle mode to shear mode in as-cast Al–2Cu, Al–3Cu and Al–5Cu alloy after ECAP processing. Also, after ECAP, small and shallow dimples were observed in the fracture surfaces. Whereas, dendrites were observed on the fracture

Published online: 17 February 2017

surface of cast samples [7]. Aal studied the effect of homogenization treatment on fracture characteristics and wear properties of ECAP processed Al–Cu alloys. It was observed that, homogenized samples showed higher mechanical properties and better wear resistance characteristics than non-homogenized samples [8]. In as-cast Zn–40Al alloy, ECAP processing led to an increase in the both the strength and the ductility [9]. Elongation to failure and tensile properties were significantly improved after rotary die equal channel angular pressing (RD-ECAP) in as-cast Al–11Si alloy [10]. The present work is motivated by the realization that in earlier investigations no attempts have been made to study the tensile properties and characteristics of the tensile fracture surfaces of ECAP processed cast Al–Zn–Mg alloys with varying zinc content. In this work, ECAP processing has been attempted on as-cast Al–5Zn–2Mg, Al–10Zn–2Mg and Al–15Zn–2Mg alloys to study the tensile properties and tensile fracture surface characteristics. All three alloys have been successfully processed up to four passes at 200 °C. Significant increase in strength and ductility have been observed after ECAP processing.

2 Experimental Materials and Procedure

Alloy compositions used in this study are presented in Table 1. The alloy was prepared by melting the commercially pure aluminium (99.7%), high purity zinc (99.9%) and high purity magnesium (99.9%) using a silicon carbide crucible in electric resistance furnace and heated to approximately 50 °C above the liquidus line of the alloy. Hexachloroethylene tablets were used to degas the melt. Coverall AR cover flux was used to avoid surface oxidation of the melt. The melt was stirred using a graphite rod and surface dross was skimmed off and the melt was poured into a metal die which was preheated to 400 °C. In order to achieve uniform distribution of alloy particles, the solidified material was remelted again. Initially, the material was cast into cylindrical rods of 25 mm diameter and 100 mm length. The chemical composition of the alloy was confirmed by using SPECTRO MAXx LMF04 optical emission spectroscopy (OES). Homogenization treatment of the cast ingots were carried out at 480 °C for 20 h and air cooled. Later, samples for ECAP were machined from homogenized material, parallel to the ingot axis, to a diameter of 16 mm and a length of 85 mm.

The ECAP processing was conducted using a die shown in Fig. 1, having an internal angle between two channels (Φ) of 120° and an angle at the outer arc of curvature (Ψ) of 30°. These angular values led to an imposed strain of approximately 0.667 on each pass through the die. The ECAP process was carried out by pressing the specimen through route B_C [11]. ECAP processing was carried out at

Table 1 Chemical composition (in wt%) of the alloys used

Alloy	Aluminium	Zinc	Magnesium
Al–5Zn–2Mg	92.4	5.09	2.07
Al–10Zn–2Mg	87.3	10.1	2.1
Al–15Zn–2Mg	82.3	15.08	2.2

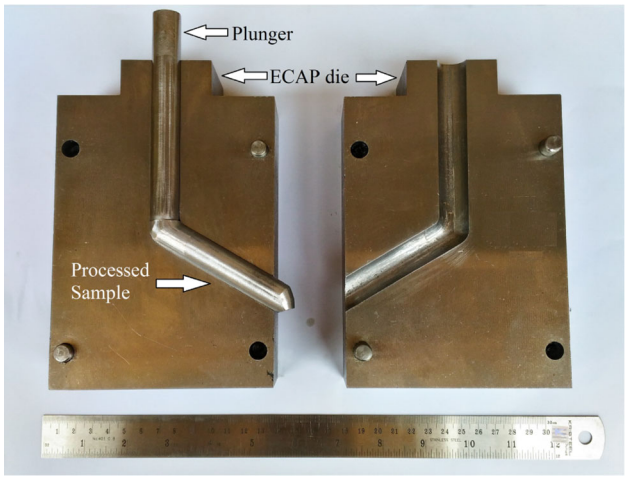

Fig. 1 Photograph of the two halves of 120° ECAP die with plunger and processed sample

200 °C and with a pressing speed approximately equal to 0.5 mm/s. To control the friction between the die and the specimen, molybdenum disulphide (MoS_2) was used as the lubricant. Prior to each pass, the die was heated up to the processing temperature (200 °C) and then the sample was inserted into the die and kept for 15 min so that the temperature equilibrium was established on the sample and the die. While processing, the whole die setup was maintained at the processing temperature using an inbuilt heater.

Optical microscopy (OM) and scanning electron microscopy (SEM) were used to study the microstructure of the material. OM images were captured by using Zeiss AX10 LAB A1 equipment and Axio Vision LE64 release 4.9.1 software. SEM images were obtained by using JEOL JSM 6380LA operating at 20 kV. For microstructure study, samples were cut perpendicular to the processed direction and metallographic technique was used to prepare the specimens and etched with Keller's reagent (2 ml of hydrofluoric acid + 3 ml of hydrochloric acid + 5 ml of nitric acid + 190 ml water). Tensile tests were conducted to evaluate the strength and ductility of the processed and unprocessed samples. Tensile tests were carried out at room temperature and at a constant cross head speed of 0.1 mm/min using Shimadzu universal testing machine AG–X plus^{TM} 100 kN equipment. The specimens before and after ECAP processing were machined to ASTM E8 standard tensile test samples and three specimens were tested to confirm the repeatability of the results. The

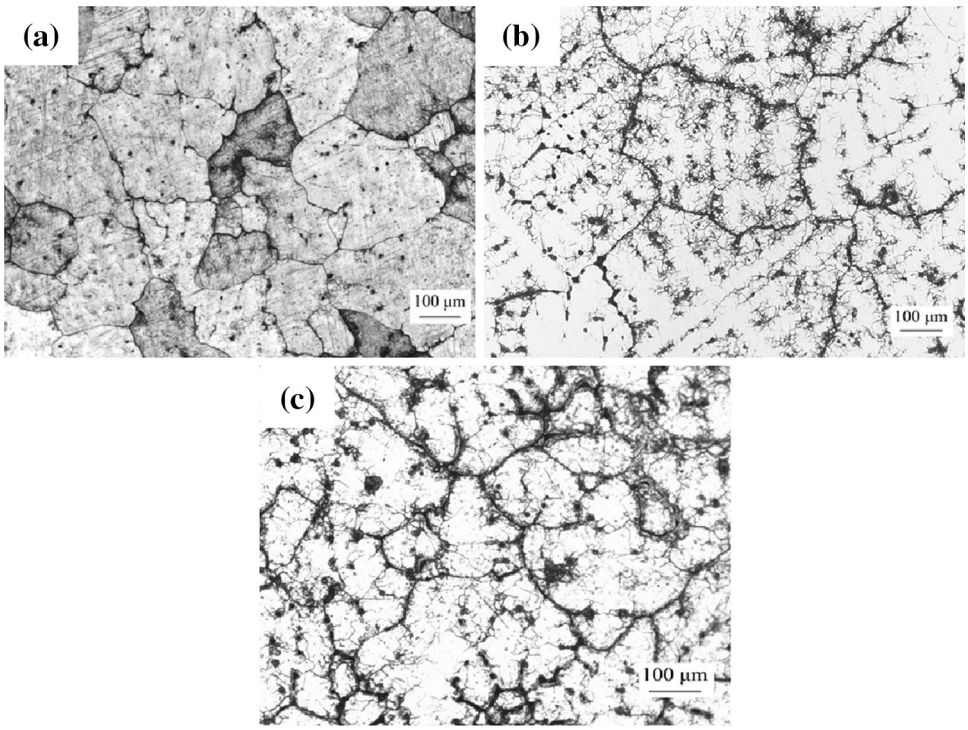

Fig. 2 OM images of the alloys in as-cast condition, **a** Al–5Zn–2Mg alloy, **b** Al–10Zn–2Mg alloy and **c** Al–15Zn–2Mg alloy

fracture surface modes were identified by visual appearance and fracture surface morphology were studied by using SEM.

3 Results and Discussion

3.1 Microstructure Evolution

Optical microscopy (OM) images of the Al–5Zn–2Mg, Al–10Zn–2Mg and Al–15Zn–2Mg alloys in as-cast condition are shown in Fig. 2. It was observed that in as-cast condition, all three alloys composed of dendritic structure and precipitates were located along the grain boundaries. These precipitates were identified as hexagonal $MgZn_2$ (η' phase) precipitates [12]. In all the three alloys, dendrites in the range of 100–200 μm size were observed. Also, with increase in the zinc content in the alloy, increase in the quantity of $MgZn_2$ precipitate was observed. It was also observed that, increase in the zinc content in the alloy led to the formation of zinc rich grain boundary layers [13]. Figure 3 shows the OM images and the SEM micrographs of Al–5Zn–2Mg, Al–10Zn–2Mg and Al–15Zn–2Mg alloys after four pass ECAP processing. It was observed that, ECAP processing led to the breakdown of the dendrites and reduction in the grain size. In Al–5Zn–2Mg alloy, after four passes, a large numbers of sub-grain boundaries and deformation bands were observed and width of these deformation bands were in the range of 2–4 μm. Similar to Al–5Zn–2Mg alloy, the Al–10Zn–2Mg alloy after four ECAP passes, was composed of sub-grain boundaries and deformation bands. The width of these deformation bands were about 5 μm. In Al–15Zn–2Mg alloy, after four ECAP passes, sub-grain boundaries of about 10 μm in size was observed.

3.2 Tensile Properties

Figure 4 illustrates the variation of the ultimate tensile strength (UTS) with the number of ECAP passes and alloy composition. ECAP processing led to a drastic improvement in the strength of the material. In the as-cast condition, the UTS of the Al–5Zn–2Mg alloy was 120 MPa. After the homogenization, a slight improvement in the UTS was observed (increased to 132 MPa). After ECAP, UTS was increased to 218 MPa in the first pass, 244 MPa in the second pass, 256 MPa in the third pass and 266 MPa in the fourth pass. After the homogenization, the UTS was increased by 10%. After the first and second ECAP pass, the UTS was increased by 82 and 103% respectively, with respect to the initial as-cast condition. After the third and fourth pass of ECAP, the UTS was increased by 113 and 122% respectively from the initial as-cast condition. In as-cast condition, the UTS of the Al–10Zn–2Mg alloy was 140 MPa. After the homogenization, a slight improvement in the UTS (increased to 156 MPa) was observed. After the ECAP, the UTS was increased to 280 MPa in the first pass, 318 MPa in the second pass, 342 MPa in the third pass and 355 MPa in the fourth pass. After the homogenization, the UTS was increased by

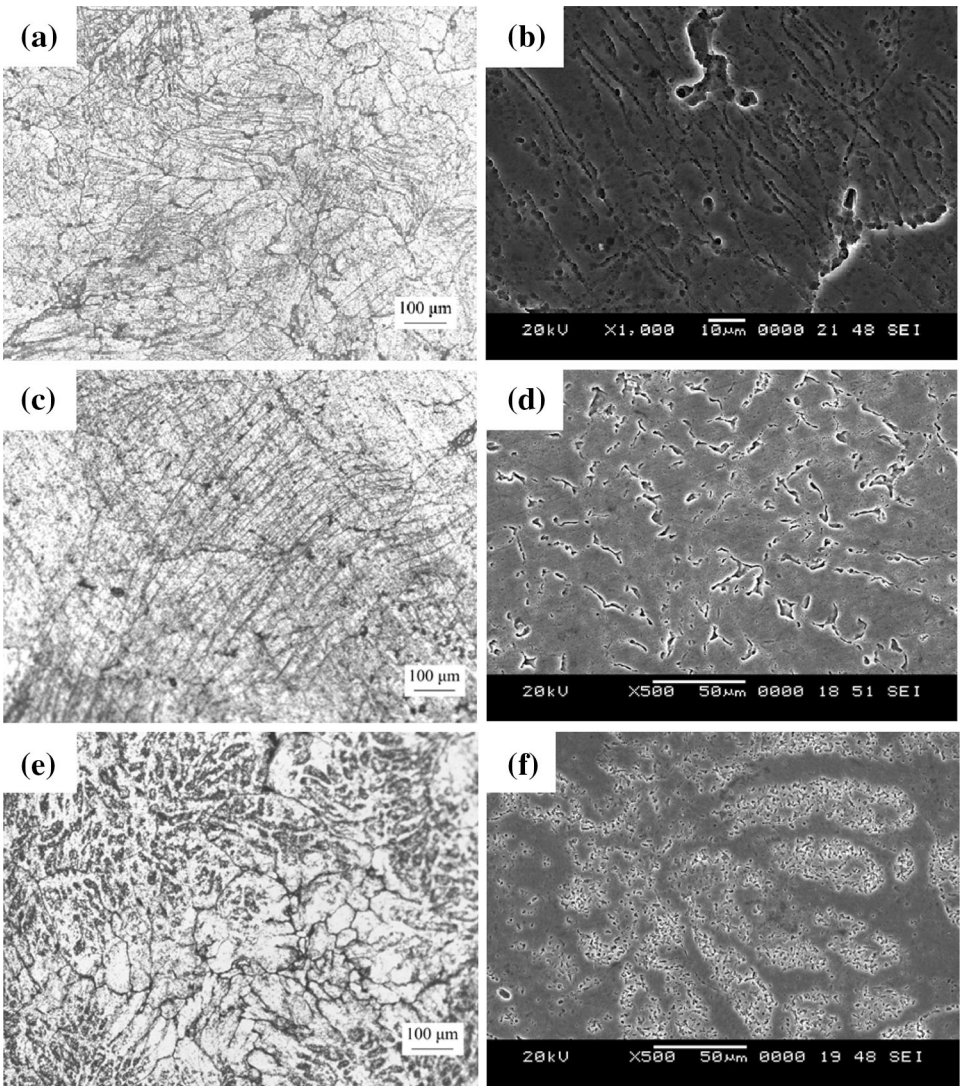

Fig. 3 OM images and SEM micrographs of the alloys after 4 pass ECAP. **a**, **b** Al–5Zn–2Mg alloy; **c**, **d** Al–10Zn–2Mg alloy and **e**, **f** Al–15Zn–2Mg alloy

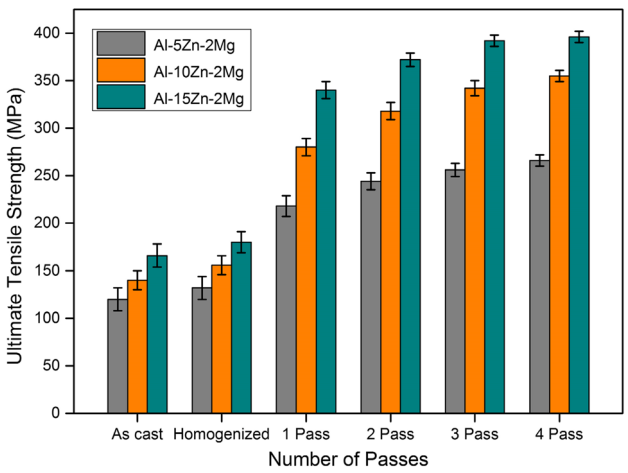

Fig. 4 Variation of ultimate tensile strength with number of ECAP passes and alloy composition

12%. The UTS was increased by 100 and 127%, after the first and second pass of the ECAP, with respect to the as-cast condition. After the third and fourth pass of the ECAP, the UTS was increased by 144 and 153% respectively, with respect to the as-cast initial condition. In as-cast condition, the UTS of Al–15Zn–2Mg alloy was 166 MPa. After the homogenization, a minor improvement in UTS (increased to 180 MPa) was observed. After ECAP process, the UTS was increased to 340 MPa in the first pass, 372 MPa the second pass, 392 MPa in the third pass and 396 MPa in the fourth pass, respectively. After the homogenization, the UTS was increased by 9% and after the first and second pass of the ECAP process, the UTS was increased by 105 and 125% respectively, with respect to the initial as-cast condition. After the third and fourth pass of the ECAP process, the UTS was increased by 136 and 139% respectively, with respect to the as-cast initial condition.

Figure 5 illustrates the variation of the yield stress (YS) with the number of ECAP passes and alloy composition. Yield stress was found out by drawing an offset line parallel to the modulus slope with 0.2% offset. The intersection point of stress–strain curve and offset line would be the yield stress value at 0.2% strain. Similar to UTS, the YS of the material increased with increasing the number of ECAP passes. Similar type of observations were made by Aal et al. [7] and Mahallawy et al. [14]. Also, the YS of the material increased with the increase in the zinc content in the material. The YS of the Al–5Zn–2Mg alloy in as-cast condition was 80 MPa. After the homogenization, YS was increased to 88 MPa. After ECAP, YS was increased to 144 MPa in the first pass, 166 MPa in the second pass, 176 MPa in the third pass and 182 MPa in the fourth pass. After first pass ECAP, large increase in YS was observed compared to the later passes. The YS of the Al–10Zn–2Mg alloy in as-cast condition was 96 MPa. After the homogenization, YS was increased to 112 MPa. After ECAP, YS was increased to 202 MPa in the first pass, 228 MPa in the second pass, 244 MPa in the third pass and 258 MPa in the fourth pass. The YS of the Al–15Zn–2Mg alloy in as-cast condition was 125 MPa. After the homogenization, YS was increased to 138 MPa. After ECAP, YS was increased to 258 MPa in the first pass, 285 MPa in the second pass, 297 MPa in the third pass and 302 MPa in the fourth pass.

Figure 6 illustrates the variation of the elongation to failure with the number of ECAP passes and alloy composition. In as-cast condition, due to the presence of dendritic structure and micro-porosity, the elongation to failure of Al–5Zn–2Mg alloy was found to be very less value (about 2.2%). After the homogenization, the elongation to failure was increased marginally to 2.8%. On the contrast, the ECAP process led to increase in the elongation to failure of the material. After ECAP process, the elongation to failure was increased to 9.2% in the first pass, 10.7% in the second pass, 11.6% in the third pass and 12.1% in the fourth pass. In as-cast condition, the elongation to failure of Al–10Zn–2Mg alloy was 1.8%. After homogenization, the elongation to failure was increased to 2.4%. After ECAP process, the elongation to failure was increased to 6.8% in the first pass, 8.1% in the second pass, 8.8% in the third pass and 9.5% in the fourth pass. In as-cast condition, the elongation to failure of Al–15Zn–2Mg alloy was about 1.3%. After the homogenization, the elongation to failure was increased to 1.8%. After the ECAP process, the elongation to failure was increased to 4.8% in the first pass, 6.2% in the second pass, 7.5% in the third pass and 7.8% in the fourth pass.

The increase in the UTS of the material could be attributed to the strain hardening and reduction in the grain size of the material. It was observed that, the UTS of the material increased with the increase in the zinc content in the material. This was due to the increase in the formation of solid solution strengthening by increasing the zinc content in the material. Addition of more zinc in the alloy increased the dislocation density in the alloy; thereby strength of the alloy also increased. It was observed that, the dislocation density increased with increase in the zinc concentration in the cast Al–Zn alloys, due to the pinning effect of zinc on dislocations [13]. It was also observed that, the strength of the alloy was increased by increasing the zinc content in the cast Al–Zn alloy processed by high pressure torsion (HPT), when the zinc content in the alloy was up to 10–15%. But the strength of the alloy was decreased, when the zinc content in the alloy was increased to 30% [13]. Similar type of observations were made in Al–Cu alloy. The strength of the material increased with increase in the copper content, while, the ductility decreased with

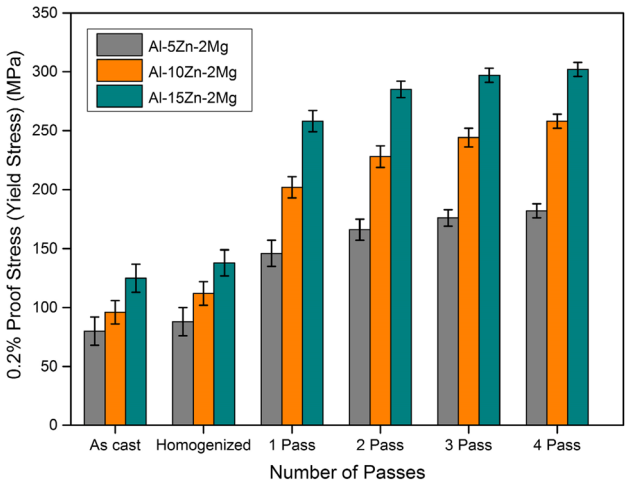

Fig. 5 Variation of yield stress with number of ECAP passes and alloy composition

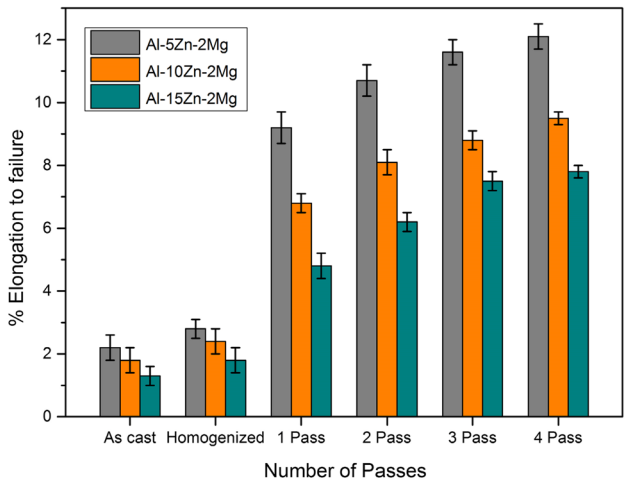

Fig. 6 Variation of elongation to failure with number of ECAP passes and alloy composition

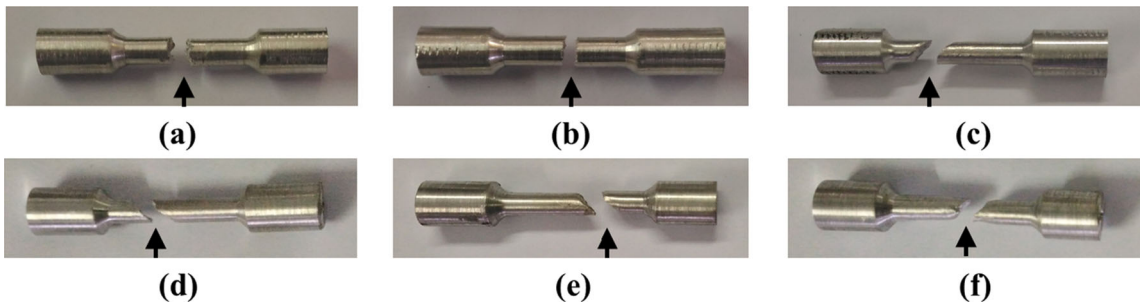

Fig. 7 Fracture modes of tensile test samples of Al–5Zn–2Mg alloy, **a** as cast, **b** homogenized, **c** 1 pass, **d** 2 pass, **e** 3 pass and **f** 4 pass

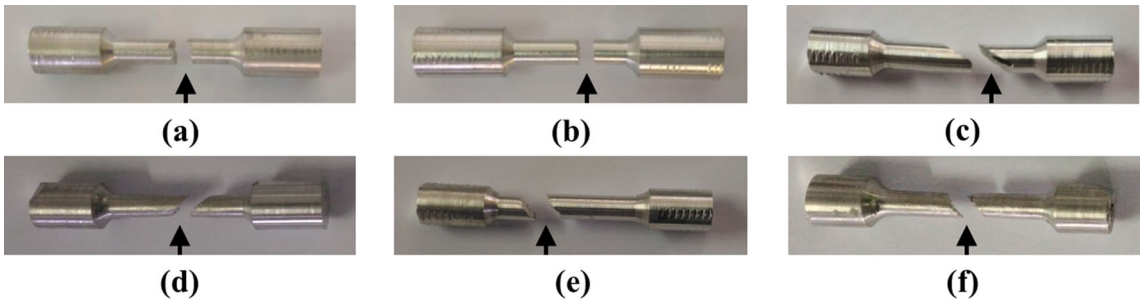

Fig. 8 Fracture modes of tensile test samples of Al–10Zn–2Mg alloy, **a** as cast, **b** homogenized, **c** 1 pass, **d** 2 pass, **e** 3 pass and **f** 4 pass

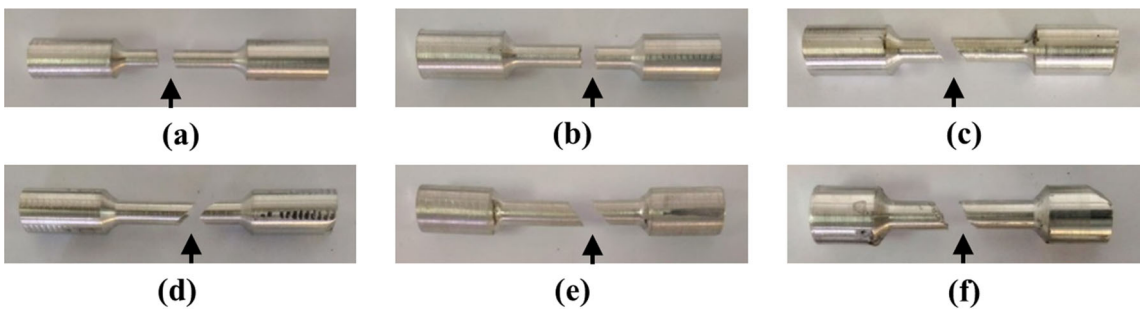

Fig. 9 Fracture modes of tensile test samples of Al–15Zn–2Mg alloy, **a** as cast, **b** homogenized, **c** 1 pass, **d** 2 pass, **e** 3 pass and **f** 4 pass

increase in the copper content [14]. In cast Al–40Zn alloy, ECAP processing led to an increase in the strength and ductility [15]. It was observed that, along with the increase in the UTS values after ECAP process, the elongation to failure was also increased. Similar type of observations were made in Al–11Si cast alloy during RD- ECAP [10]. The increase in the elongation to failure with the ECAP passes was due to the transformation of the material from brittle nature to ductile nature. Increase in the ductility after ECAP could be attributed to the formation of more homogeneous microstructure. It was observed that, elongation to failure of the material decreased with increase in the zinc content in the material. Increase in the elongation to failure with the number of passes was observed in ECAP of cast Al–3Cu alloy by Aal [16]. Increase in the strength and overall elongation to failure was observed in ECAP of Al–Zn–Mg alloys after 4 passes [17].

3.3 Fracture Mode and Fracture Surface Morphology

Figure 7 shows the tensile test samples of Al–5Zn–2Mg alloy in various conditions. In as-cast and homogenized conditions, the fracture occurred normal to the axis of the specimen. This is shown in Fig. 7a and b, respectively. Brittle fracture mode was observed in the as-cast and homogenized tensile test samples. In as-cast tensile samples, plastic deformation was difficult under tensile test [18]. The fracture could be explained by the distribution of

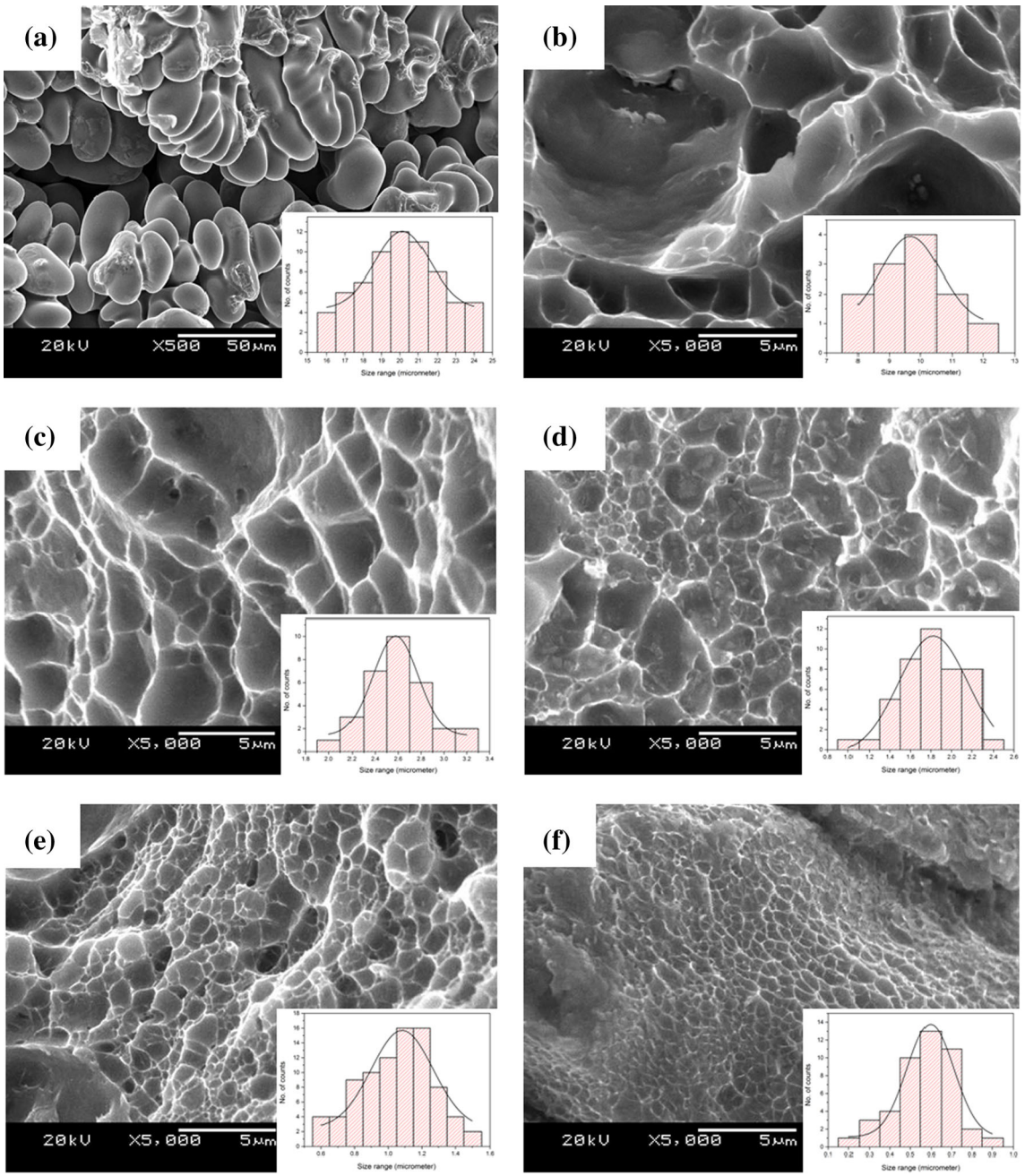

Fig. 10 SEM micrographs of the fracture surfaces after tensile testing of Al–5Zn–2Mg alloy, **a** as cast, **b** homogenized, **c** 1 pass, **d** 2 pass, **e** 3 pass and **f** 4 pass

the second phase particles. In as-cast condition, the second phase particles were distributed along the grain boundaries. These second phase particles obstructed the grain deformation during the tensile test. The second phase particles while disengaging from the grain boundary formed micropores which grew continuously to initiate the crack, leading to fracture. Therefore, the fracture occurred normal to the load direction [16]. After the first pass of the ECAP process, the fracture mode was transformed to shear mode with a fracture angle approximately equal to 45° with respect to the tensile axis as shown in Fig. 7c. This was due to strong strain-hardening effect during ECAP processing [19]. Also, with the increase in the ECAP passes, the strain-hardening degree gradually increased [18]. With the increase in the number of ECAP passes, the fracture appearance continued to show the shear fracture mode. This has been indicated in images presented in Fig. 7d–f corresponding to second pass, third pass and fourth pass, respectively. The fracture angles were very close to 45° with respect to the tensile axis. In the ECAP processed

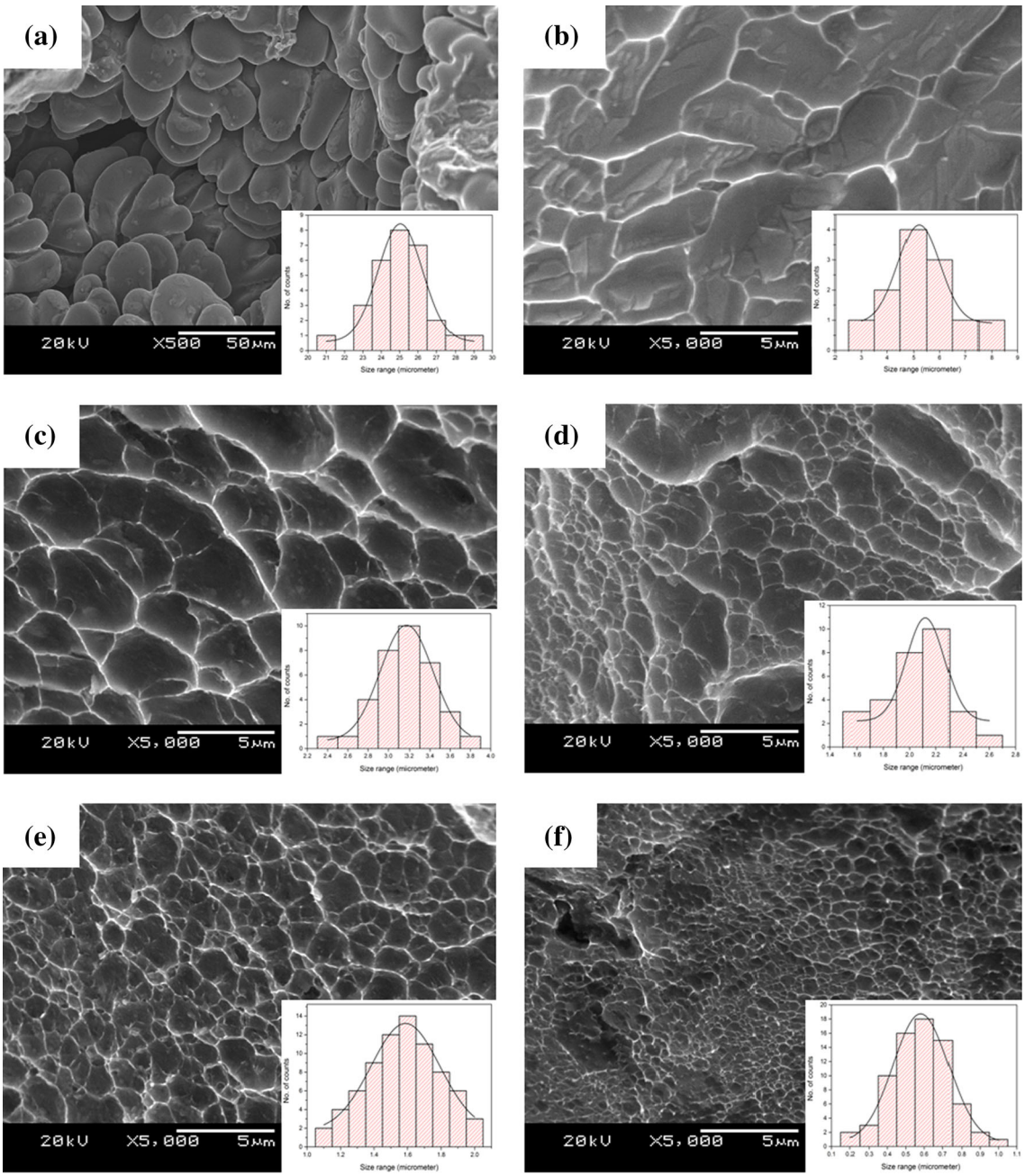

Fig. 11 SEM micrographs of the fracture surfaces after tensile testing of Al–10Zn–2Mg alloy, **a** as cast, **b** homogenized, **c** 1 pass, **d** 2 pass, **e** 3 pass and **f** 4 pass

samples, due to intense shearing, the second phase particles fragmented in the shear plane [18]. Normally, the plane containing second phase particles were weaker. Consequently, fracture would occur in the shear plane during tensile testing of ECAP processed samples [18]. It was observed that, samples subjected to ECAP processing always failed in a shear fracture mode in tensile testing [19]. Similar behaviour occurred in the Al–10Zn–2Mg alloy and Al–15Zn–2Mg alloy tensile test samples, before and after ECAP processing as shown in Figs. 8 and 9 respectively.

SEM micrographs of the fracture surface morphologies of the tensile test samples of Al–5Zn–2Mg alloy in various conditions are shown in Fig. 10. In as-cast condition, the fracture surface was composed of micro-porosities and dendrite structure; dimples were not observed (Fig. 10a). In this condition, dendrites of 20 µm were observed. After the homogenization, dendritic structures and micro-

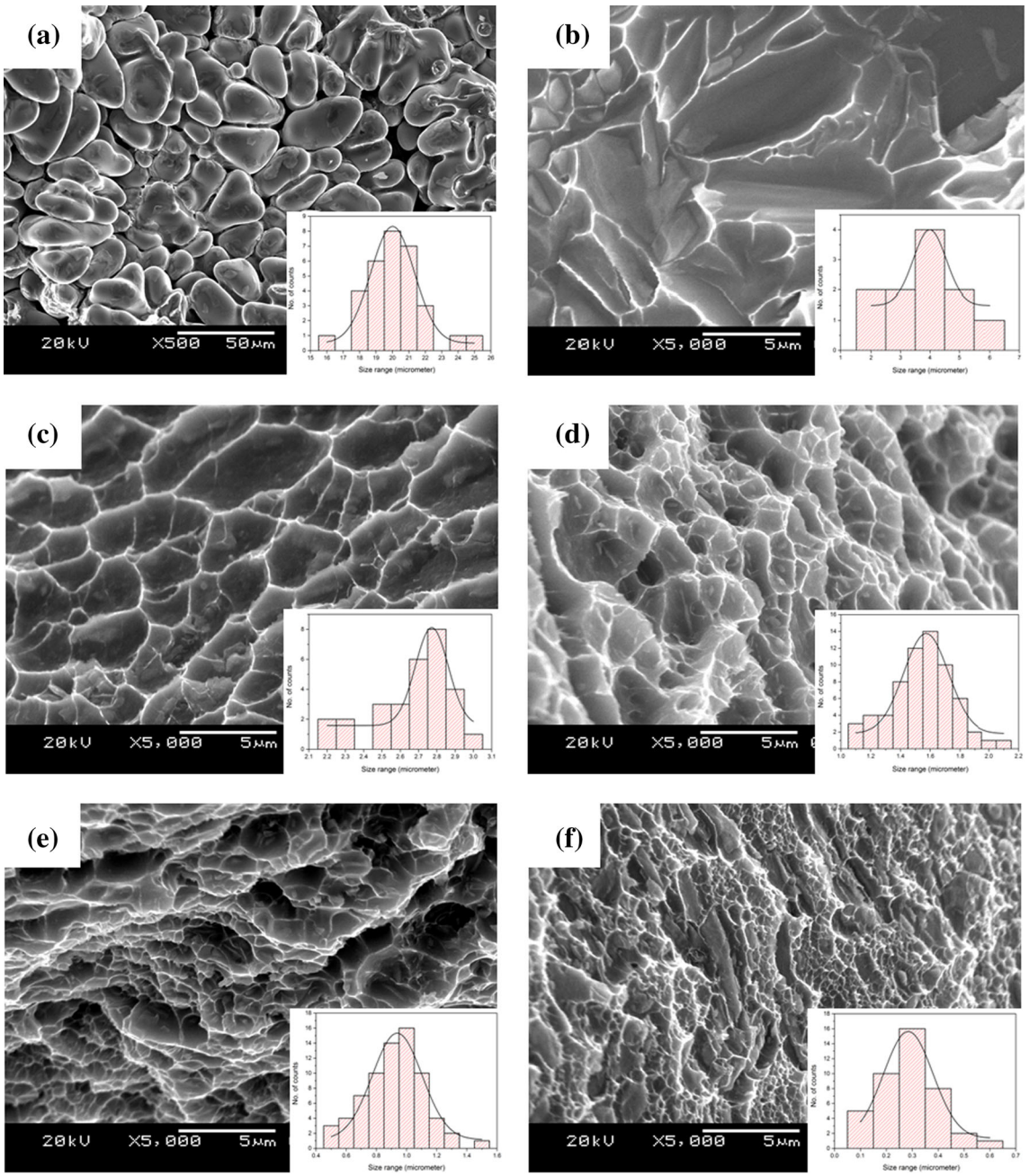

Fig. 12 SEM micrographs of the fracture surfaces after tensile testing of Al–15Zn–2Mg alloy, **a** as cast, **b** homogenized, **c** 1 pass, **d** 2 pass, **e** 3 pass and **f** 4 pass

porosities which were observed in the cast condition disappeared from the fracture surface. Large dimples with diameter of approximately 10 µm were observed. After the ECAP process, the dimple size decreased and showed a homogeneous distribution across the fracture surfaces. It was also observed that dimples in the fracture surfaces were shallower than those before ECAP process and dimple size was reduced with the increase in the number of ECAP passes. The average size of the dimples in the fracture surfaces were reduced to 2.5, 1.8, 1.2 and 0.6 µm in the first pass, second pass, third pass and fourth pass respectively. The reduction in the dimple size was attributed to the reduction in the grain size. Similar observations were reported in the previous works carried on cast aluminium and cast Al–Cu alloy by Aal et al. [7] and Al–Zn alloy by Saray and Purcek [15]. The continuous reduction in dimple size could be related to grain refinement as well as strain hardening and the fragmentation of second phase particles was caused by ECAP [20].

Figure 11 shows the SEM micrographs of the fracture surface morphologies of the tensile test samples of Al–10Zn–2Mg alloy under various conditions. Similar type of observations were seen in the tensile fracture samples of Al–10Zn–2Mg alloy with reference to the Al–5Zn–2Mg alloy. In as-cast condition, dendrites of 25 μm were observed. After the homogenization, dimples of diameter approximately equal to 5 μm were observed. After the ECAP process, the average size of the dimples in the fracture surfaces were reduced to 3.2, 2.2, 1.6 and 0.6 μm in the first pass, second pass, third pass and fourth pass respectively. Figure 12 shows the SEM micrographs of the fracture surface morphologies of the tensile test samples of Al–15Zn–2Mg alloy under various conditions. A similar observation was seen in the tensile fracture samples of Al–15Zn–2Mg alloy with reference to the Al–5Zn–2Mg alloy and Al–10Zn–2Mg alloy. In as-cast condition, dendrites of 20 μm were observed. After homogenization, dimples of diameter of 4 μm size were observed. After the ECAP process, the average size of the dimples in the fracture surfaces were reduced to 2.8, 1.6, 1 and 0.3 μm in the first pass, second pass, third pass and fourth pass respectively.

4 Conclusions

The Al–Zn–Mg alloy system turns out to be a very interesting model system to study enhancement in tensile properties developed by SPD and their link with grain refinement. The Al–5Zn–2Mg, Al–10Zn–2Mg and Al–15Zn–2Mg alloys were processed successfully up to 4 passes in route B_C at 200 °C. The main outcomes of this study are summarized as follows.

- After ECAP, deformation bands in the range of 2 to 4 μm in Al–5Zn–2Mg alloy and 5 μm in Al–10Zn–2Mg alloy were observed. While in Al–15Zn–2Mg alloy, sub-grains of about 10 μm size was observed.
- After ECAP processing, significant increase in the UTS and the elongation to failure were observed. After 4 passes, the UTS was increased to 266 MPa, 355 MPa and 396 MPa in Al–5Zn–2Mg, Al–10Zn–2Mg and Al–15Zn–2Mg alloys, from the initial as-cast condition values of 120 MPa, 140 MPa and 166 MPa, respectively. Elongation to failure increased to 12.1, 9.5 and 7.8% in Al–5Zn–2Mg, Al–10Zn–2Mg and Al–15Zn–2Mg alloys, from the initial as-cast condition values of 2.2, 1.8 and 1.3%, respectively.
- The fracture mode was transformed from brittle mode to shear mode after ECAP processing in all the three alloys. In cast condition, the fracture surface was composed of dendrites and micro-porosities. Dendrites of 20, 25 and 20 μm in size were observed in Al–5Zn–2Mg, Al–10Zn–2Mg and Al–15Zn–2Mg alloys, respectively. After 4 passes, small dimples of 0.6, 0.6 and 0.3 μm in size were observed in Al–5Zn–2Mg, Al–10Zn–2Mg and Al–15Zn–2Mg alloys, respectively.

References

1. Valiev R Z, Islamgaliev R K, and Alexandrov I V, *Prog Mater Sci* **45** (2000) 103.
2. Langdon T G, Furukawa M, Nemoto M, and Horita, *Jom* **52** (2000) 30.
3. Segal V M, Raznikov V I, Drobyshewsky A E, and Kopylov V I, *Russian Metallurgy* 1 (1981) 99.
4. Zehetbauer Y T, and Zhu M J, *Bulk Nanostrucutred Materials*, Wiley-VCH, Weinheim (2009).
5. Shaeri M H, Salehi M T, Seyyedein S H, Abutalebi M R, and Park J K, *Mater. Des.* **57** (2014) 250.
6. Prados E, Sordi V, and Ferrante M, *Mater. Sci. Eng. A* **503** (2009) 68.
7. El Aal M I A., El Mahallawy N, Shehata F A, El Hameed M A, Yoon E Y, Lee, J H, & Kim H S, *Met. Mater. Int.* **16** (2010) 709.
8. El Aal M I A, *Mater. Sci. Eng. A* **539** (2012) 308.
9. Purcek G, Saray O, Karaman I, and Kucukomeroglu T, *Mater. Sci. Eng. A* 490 (2008) 403.
10. Ma A, Saito N, Takagi M, Nishida Y, Iwata H, Suzuki K, Shigematsu I, and Watazu A, *Mater. Sci. Eng. A* **395** (2005) 70.
11. Nakashima K, Horita Z, Nemoto M, and Langdon T G, *Mater. Sci. Eng. A* **281** (2000) 82.
12. Zhang S, Hu W, Berghammer R, and Gottstein G, *Acta Mater.* **58** (2010) 6695.
13. Chinh N Q, Jenei P, Gubicza J, Bobruk E V, Valiev R Z, and Langdon T G, *Mater. Lett.* **186** (2017) 334.
14. El Mahallawy N, Shehata F A, El Hameed M A, and El Aal M I A, *Mater. Sci. Eng. A* **517** (2009) 46.
15. Saray O, and Purcek G, *J. Mater. Process. Technol.* **209** (2009) 2488.
16. El Aal M I A, *Mater. Sci. Eng. A,* **528** (2011) 6946.
17. Duan Z C, Chinh N Q, Xu C, and Langdon T G, *Metall. Mater. Trans. A* **41** (2010) 802.
18. Fang D R, Zhang Z F, Wu S D, Huang C X, Zhang H, Zhao N Q and Li J J, *Mater. Sci. Eng. A* **426** (2006) 305.
19. Fang D R, Duan Q Q, Zhao N Q, Li J J, Wu S D and Zhang Z F, *Mater. Sci. Eng. A* **459** (2007) 137.
20. Vinogradov A, Ishida T, Kitagawa K and Kopylov V I, *Acta Mater.* **53** (2005) 2181.